LETTER

doi:10.1038/nature12567

Calving fluxes and basal melt rates of Antarctic ice shelves

M. A. Depoorter[1], J. L. Bamber[1], J. A. Griggs[1], J. T. M. Lenaerts[2], S. R. M. Ligtenberg[2], M. R. van den Broeke[2] & G. Moholdt[3]

Iceberg calving has been assumed to be the dominant cause of mass loss for the Antarctic ice sheet, with previous estimates of the calving flux exceeding 2,000 gigatonnes per year[1,2]. More recently, the importance of melting by the ocean has been demonstrated close to the grounding line and near the calving front[3–5]. So far, however, no study has reliably quantified the calving flux and the basal mass balance (the balance between accretion and ablation at the ice-shelf base) for the whole of Antarctica. The distribution of fresh water in the Southern Ocean and its partitioning between the liquid and solid phases is therefore poorly constrained. Here we estimate the mass balance components for all ice shelves in Antarctica, using satellite measurements of calving flux and grounding-line flux, modelled ice-shelf snow accumulation rates[6] and a regional scaling that accounts for unsurveyed areas. We obtain a total calving flux of 1,321 ± 144 gigatonnes per year and a total basal mass balance of −1,454 ± 174 gigatonnes per year. This means that about half of the ice-sheet surface mass gain is lost through oceanic erosion before reaching the ice front, and the calving flux is about 34 per cent less than previous estimates derived from iceberg tracking[1,2,7]. In addition, the fraction of mass loss due to basal processes varies from about 10 to 90 per cent between ice shelves. We find a significant positive correlation between basal mass loss and surface elevation change for ice shelves experiencing surface lowering[8] and enhanced discharge[9]. We suggest that basal mass loss is a valuable metric for predicting future ice-shelf vulnerability to oceanic forcing.

Antarctica gains mass from snow accumulation in its interior and loses mass through ice discharge across the grounding line and into the ocean, where ice shelves form. These floating shelves are crucial to the stability of the ice sheet because they buttress the grounded ice upstream[10]. Loss of buttressing from ice-shelf thinning or removal leads to enhanced discharge of inland ice[11] and may be triggered by oceanic[8] and atmospheric[12] warming.

Calving fluxes for the whole of Antarctica have been inferred from temporally and spatially limited ship-based campaigns and satellite tracking from the US National Ice Center[1,2,7]. These calculations relied on many assumptions about the volume, density and lifetime of icebergs[1]. In 1992, the total calving flux was calculated to be 2,016 ± 672 Gt yr^{-1} (ref. 1), in agreement with the mean of 12 previous estimates from the 1970s and 1980s. Combining estimates of snow accumulation at the surface of the ice sheet and subshelf melt rates, this led to the conclusion that Antarctica was losing more than 1.3 mm yr^{-1} in sea-level equivalent as a result of enhanced iceberg calving[1,2]. In the absence of better estimates, recent studies of the hydrographic effects[7] of, and iron fluxes[13] from, icebergs in the Southern Ocean have used these figures (Supplementary Discussion 1).

Melting of ice shelves in Antarctica is caused by three different modes of relatively warm-water circulation[1]. The first mode is related to sea-ice formation and production of high-salinity shelf water that reaches the grounding line and forms ice-shelf water (ISW), a mix of high-salinity shelf water and fresh water. The second mode is due to the incursion of circumpolar deep water into the ice-shelf cavity, and the third mode is due to tidal and wind-induced mixing near the ice-shelf edge. Between the grounding line and the ice-shelf edge, refreezing takes place as the rising plume of ISW becomes supercooled and precipitates frazil ice (mode 1). This results in melting under ice shelves being most prevalent at the grounding line and close to the calving front[3–5,14]. Melt rates under Antarctic ice shelves have been inferred from glaciological studies[3], water measurements underneath[15] and in front of ice shelves, modelling studies[16], and compilations of different approaches[1]. Whereas glaciological studies are limited to a few ice-shelf locations, oceanographic studies lack temporal and spatial resolution. Modelling studies have provided important knowledge on ice–ocean interactions[16] but still have considerable uncertainties owing to a paucity of oceanographic and sub-ice-shelf geometry data[1,17], poorly resolved basal accretion[18], and grid resolution limitations[18].

Detailed studies of ice-shelf mass fluxes have provided improved estimates of the mass balance for a few targeted ice shelves[5,14], but so far no study has undertaken this rigorously across the whole of Antarctica. Here we calculate calving fluxes from ice thickness, derived directly from either our analysis of satellite radar altimeter measurements of freeboard[19] (ice-shelf elevation above mean sea level) or from ice-penetrating radar (IPR) data (32% by the first technique and 68% by the second). The altimetry is combined with corrections for changes in elevation between 1995 and 2009, and for firn air content and compaction obtained from our regional climate model[6] (Supplementary Discussion 2). We do this for all ice shelves exceeding 100 km^2 in size and combine the derived thicknesses with ice surface velocity from synthetic-aperture radar interferometry[20] (InSAR). The grounding-line fluxes (GLFs) are then obtained in combination with a new grounding-line data set. Although we do not focus here on the mass balance of the grounded ice sheet, it is interesting to note that the difference between our GLF and grounded surface mass balance (SMB) is −66 Gt yr^{-1}. This is, unlike previous mass budget estimates, very close to a recent assessment, from the GRACE satellite mission, of −69 Gt yr^{-1} for the period 2002–2010[21].

The basal mass balance (BMB) is determined, assuming conservation of mass, from the difference between the GLF and the SMB, and the calving flux (CF). Ice-shelf thinning rates[8] are added to BMB to account for non-steady-state behaviour (Table 1). We account for unsurveyed shelves using a physically based regional upscaling of our results (Supplementary Discussion 3). We find that for Antarctica as a whole, mass loss is roughly equally split between basal mass loss (the sum of total melt and accretion) and calving. Locally, however, the melt ratio (MR = |BMB|/[CF + |BMB|]) varies considerably, from ~10% to ~90% (Fig. 1). For the fringing ice shelves of West Antarctica, it is 74% (Table 1). Thus, for the Bellingshausen Sea and Amundsen Sea sectors, about two-thirds of the mass loss is via BMB. In contrast, the average melt ratio for the rest of Antarctica is 40%, and for the two largest ice shelves, the Filchner-Ronne and the Ross, the ratio is just 17%. These two ice shelves are consequently responsible for one-third of the iceberg production in Antarctica.

[1]Bristol Glaciology Centre, School of Geographical Sciences, University of Bristol, Bristol BS8 1SS, UK. [2]Institute for Marine and Atmospheric Research Utrecht, Utrecht University, 3584 CC Utrecht, The Netherlands. [3]Scripps Institution of Oceanography, University of California San Diego, La Jolla, California 92093, USA.

Table 1 | Mass balance of Antarctic ice shelves by oceanic sector

Ocean sector	Ice shelves	GLF (Gt yr^{-1})	SMB (Gt yr^{-1})	CF (Gt yr^{-1})	dh/dt (Gt yr^{-1})	BMB (Gt yr^{-1})	Ice-shelf area (10^3 km^2)	SBMB (m yr^{-1})	MR (%)
West Indian Ocean	AR, NE, AIS, W*	235 ± 30	49 ± 8	155 ± 22	−11 ± 8	−140 ± 38	174	−0.80 ± 0.22	47
West Indian Ocean+		324 ± 31	—	204 ± 29	—	−179 ± 43	—	—	47
East Indian Ocean	SHA*, VAN, TOT*,	333 ± 16	48 ± 7	213 ± 44	−51 ± 20	−219 ± 48	65	−3.35 ± 0.73	51
East Indian Ocean+	MU, POR*, ADE*,MER, NIN, COO, REN*	508 ± 26	—	306 ± 75	—	−300 ± 80	—	—	50
Ross Sea	DRY, RIS, SUL,	149 ± 16	71 ± 17	153 ± 10	0 ± 0	−67 ± 26	492	−0.14 ± 0.05	30
Ross Sea+		175 ± 16	—	167 ± 15	—	−79 ± 28	—	—	32
Amundsen Sea	LAN*, GET*, CD*,	383 ± 19	55 ± 11	198 ± 43	−156 ± 13	−395 ± 48	56	−7.11 ± 0.87	67
Amundsen Sea+	THW*, PI*, COS	505 ± 24	—	232 ± 50	—	−484 ± 57	—	—	68
Bellingshausen Sea	ABB*, VEN*, GEO*,	139 ± 11	82 ± 16	31 ± 10	−65 ± 43	−255 ± 22	86	−2.98 ± 0.26	89
Bellingshausen Sea+	WOR	174 ± 12	—	41 ± 13	—	−281 ± 23	—	—	87
Weddell Sea	LBC, FRIS, BRL, JFL	334 ± 35	139 ± 23	355 ± 31	0 ± 0	−118 ± 52	608	−0.19 ± 0.09	25
Weddell Sea+		363 ± 35	—	371 ± 33	—	−131 ± 53	—	—	26
Fringing West Antarctica	SUL, LAN*, GET*,	542 ± 23	147 ± 19	232 ± 54	−221 ± 45	−678 ± 53	154	−4.40 ± 0.35	74
Fringing West Antarctica+	CD*, THW*, PI*, COS*, ABB*, VEN*, GEO*, WOR	700 ± 27	—	275 ± 63	—	−792 ± 62	—	—	74
Total surveyed	—	1,573 ± 56	444 ± 36	1,106 ± 141	−282 ± 50	−1,193 ± 163	1,481	−0.81 ± 0.11	52
Total upscaling	—	476 ± 67	—	216 ± 33	—	-261 ± 34	74	−3.53 ± 0.47	55
Total Antarctica	—	2,049 ± 87	—	1,321 ± 44	—	−1,454 ± 174	1,555	−0.94 ± 0.11	52

See Fig. 1 for ice-shelf names and Supplementary Table 1 for the data here as tabulated for individual ice shelves. A plus sign indicates that regional upscaling is included. dh/dt, non-steady-state mass change. Uncertainty estimates, 1 s.d.
* Corrected for imbalance using ICESat (NASA's Ice, Cloud, and land Elevation Satellite) elevation rates.

The greatest basal mass loss does not come from the largest ice shelves, but from medium- to small-sized ones such as George VI, Getz, Totten and Pine Island (Fig. 1). Representing 91% of the ice-shelf area, the ten largest ice shelves produce only ~50% of the basal mass loss for Antarctica. Studies focusing on a small number of large ice shelves (four to ten) are therefore not representative of the continent as a whole[1,17]. Our total BMB, of −1,454 ± 174 Gt yr^{-1}, is of the same order of magnitude as estimates from oceanographic measurements and modelling[1,17,18,22] (~500–1,600 Gt yr^{-1}), but we find large regional differences. For example, a finite-element mesh ice–ocean model yields larger numbers for most of the ice shelves considered, especially the largest ones[18] (Supplementary Table 2). This is despite not taking into account the tidal effect on melting at the calving front, which is an important factor in the overall ice-shelf mass balance[3,5]. This overestimation seems partly to stem from very low accretion rates[18] (an order of magnitude lower than estimates based on observations for most parts of the Filchner-Ronne Ice Shelf accretion zone[5]). Different atmospheric forcings explain most of the large discrepancies between different model simulations[17,18,22] (H. Hellmer, personal communication). However, our results for the BMB agree well with previous estimates using a similar methodology[14,23] (Supplementary Discussion 4).

The mean specific BMB (SBMB = BMB per unit area) for all ice shelves is −0.81 ± 0.11 m yr^{-1} (water equivalent), but it varies from −0.07 to −15.96 m yr^{-1} between ice shelves (Fig. 2 and Supplementary Table 1). The SBMB is strongly negative (more than 2.00 m yr^{-1} in magnitude) for all ice shelves fringing West Antarctica (SUL, LAN, GET, CD, THW, PI, COS, ABB, VEN, GEO and WOR) and in clustered parts of East Antarctica, that is, Wilkes Land (VAN, TOT, MU, POR and ADE) and Enderby Land (NE and SHA). The SBMB is relatively small (less than 1.00 m yr^{-1} in magnitude) mainly for the large ice shelves (LBC, FRIS, BRL, JF, AR, AIS and RIS), and this could be due to substantial bottom-ice accretion compensating for strong melting near the grounding line. In forming and depositing buoyant frazil ice crystals, the rising ISW benefits from troughs and cavities in the subshelf topography, which are formed downstream of peninsulas and ice rises for the Filchner-Ronne[5], Amery[24], Larsen B and Larsen C[25]

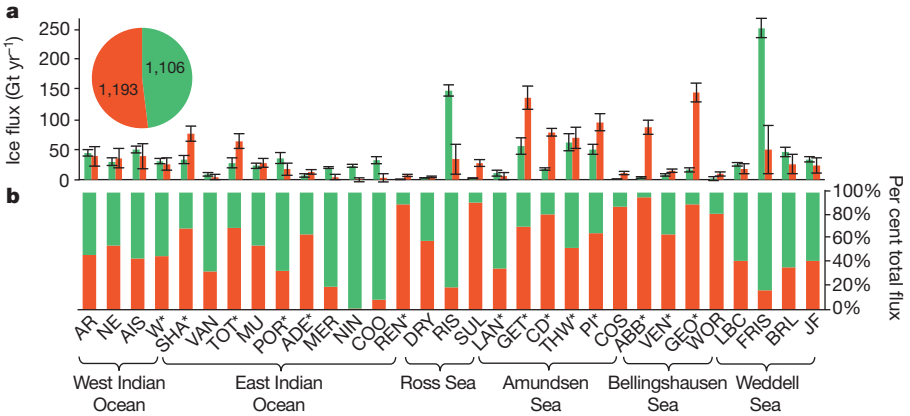

Figure 1 | Basal mass loss and calving fluxes of Antarctic ice shelves. **a**, Calving fluxes (green) and basal mass loss (−BMB; red). Pie chart shows numbers for surveyed ice shelves only. Errors, 1 s.d. **b**, Ratio between calving flux (green) and BMB (red), in per cent of total flux. Ice shelves are ordered clockwise geographically, starting from longitude 0°. Ice-shelf names: AR, Astrid-Ragnhild; NE, Northeast; AIS, Amery; W, West; SHA, Shackleton; VAN, Vanderford; TOT, Totten; MU, Moscow University; POR, Porpoise; ADE, Adélie; MER, Mertz; NIN, Ninnis; COO, Cook; REN, Rennick; DRY, Drygalski; RIS, Ross; SUL, Sulzberger; LAN, Land; GET, Getz; CD, Crosson and Dotson; THW, Thwaites; PI, Pine Island; COS, Cosgrove; ABB, Abbot; VEN, Venable; GEO, George VI; WOR, Wordie; LBC, Larsen B and Larsen C; FRIS, Filchner-Ronne; BRL, Brunt and Riiser-Larsen; JF, Jelbart and Fimbul. Asterisks indicate basins experiencing dynamic thinning[9] and ice shelves experiencing thinning[8]. See Supplementary Fig. 1 for mapped melt ratios. The brackets underneath indicate oceanic sectors.

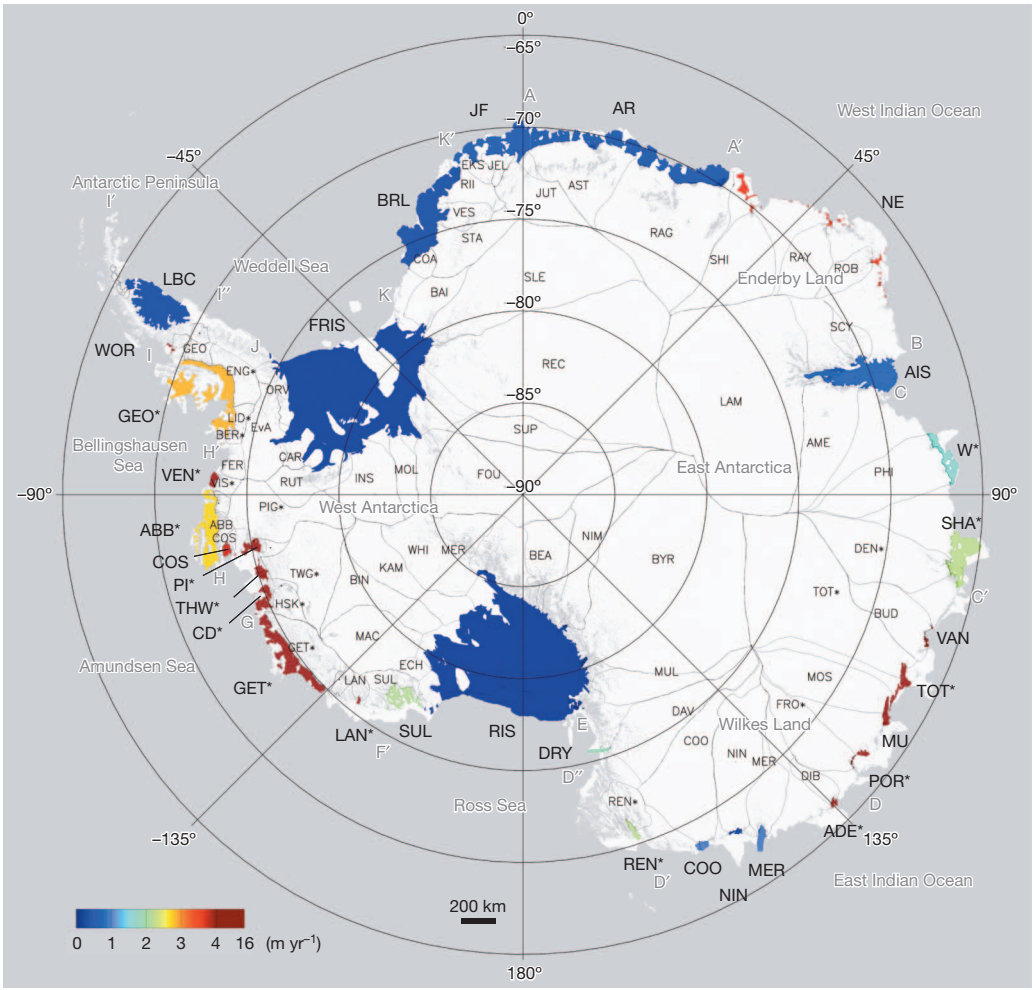

Figure 2 | Mean basal mass-loss rates of Antarctic ice shelves. Ice shelves are colour-coded for area averaged basal mass loss. Drainage basins feeding the respective ice shelves are indicated using thin black lines. Grey labels indicate oceanic sectors and major basins.

ice shelves. For smaller ice shelves, the ISW plume will not be able to precipitate and deposit marine ice to the same degree, because the subshelf topography is more homogenous and the grounding-line melt zone is closer to the ice front.

The Filchner-Ronne and Ross ice shelves have similar areas of continental shelf[3] where high-salinity shelf water forms, grounding-line lengths of ~5,100 km and respective areas of 423×10^3 and 477×10^3 km^2, integrated SMBs of 70 and 61 Gt yr^{-1} and SBMBs of −0.12 and −0.07 m yr^{-1}. Similar SBMBs indicate that the higher grounding-line melt rate on Filchner-Ronne relative to Ross, because of a deeper grounding line[4], is balanced by higher marine-ice accretion. Thus, there is relatively little marine-ice accumulation found underneath Ross[26] by comparison with the large volume under Filchner-Ronne[5].

Basal mass loss is spread quite evenly between the six oceanic sectors (131–300 Gt yr^{-1}) except for the Ross Sea and Amundsen Sea regions (79 and 484 Gt yr^{-1}, respectively) (Fig. 1 and Table 1). About 30% of all Antarctic icebergs, by mass, are formed in the Weddell Sea sector (371 Gt yr^{-1}) and only 3% are formed in the Bellingshausen Sea (41 Gt yr^{-1}). This large volume of icebergs is exported from the Weddell Sea, along the Antarctic Peninsula and into the Scotia Sea (forming the 'iceberg alley'). This may explain the increased concentration of iron maintained in the Scotia Sea as well as its high productivity compared with the mainly high-nutrient, low-chlorophyll Southern Ocean[27]. The western coastal current in combination with the geometry of the Antarctic Peninsula provides unique conditions for efficient iceberg export away from the Antarctic coast[7].

Comparing our SBMB with surface lowering rates[8] from ICESat (NASA's Ice, Cloud, and land Elevation Satellite), we find that a large negative SBMB seems to be a good indicator of ice-shelf vulnerability to oceanic forcing (Fig. 3): in this case, the incursion of warm circumpolar deep water through deep troughs. This implies that other fringing ice shelves with large negative SBMB (more than 2.00 m yr^{-1} in

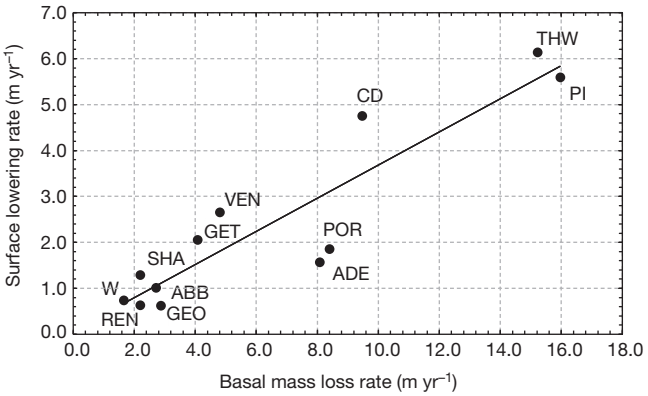

Figure 3 | Ice-shelf surface lowering rates versus mean basal mass-loss rates. We find a significant correlation ($R^2 = 0.84$ (coefficient of determination); $P = 3.13 \times 10^{-5}$; F-test) between surface lowering rates[8] and our mean basal mass-loss rates (−SBMB) for thinning ice shelves. All 12 ice shelves with a significant and extensive surface lowering rate are included.

magnitude), such as the Northeast, Vanderford, Moscow University, Totten, Sulzberger, Land and Cosgrove ice shelves (Fig. 2), could have a similar vulnerability to oceanic forcing.

Freshwater fluxes enter the Southern Ocean by different paths. Whereas basal melt water is distributed over the upper few hundred metres of the coastal water column, icebergs drift and melt farther away from the continent. Having good constraints on these fluxes and their distribution will improve our understanding of Antarctic deep-water formation and of the hydrography of the Southern Ocean. Our results will also help constrain the controls on the primary productivity of the Southern Ocean via iron fertilization[13], because bottom melt water has been linked to phytoplankton blooms[28] and melting icebergs are considered hotspots for marine life[29]. Quantifying the relative importance of bottom melt and iceberg calving is also crucial for accurately modelling the formation of sea ice. Indeed, ISW has a stabilizing effect on the water column in front of ice shelves and favours the formation of sea ice[17], whereas icebergs promote convection and mixing[7]. The poor agreement, regionally, with ice–ocean–atmosphere models indicates that further work is required before these can faithfully reproduce observed patterns of BMB and freshwater production.

METHODS SUMMARY

We use standard budget methods to calculate the BMB for each ice shelf in Antarctica: 0 = BMB + SMB + GLF − CF. We determine BMB as the remaining unknown in the mass balance equation, assuming a steady-state front position but accounting for ice-shelf imbalance using surface elevation changes from ICESat. Calving flux is found by integrating ice-shelf thickness and ice velocity along the calving front (Supplementary Discussion 6 and Supplementary Fig. 2). Our ice-shelf thickness is based on altimetry data from the European Remote-sensing Satellite (ERS-1) for 1994–1995, and is supplemented by ICESat data for latitudes south of the ERS-1 limit for 2003–2009[19]. Elevation data are corrected to the year 2009 using elevation rates from ERS-1[30] (1994–2002) and from ICESat[8] (2003–2009) to fit velocity and IPR data sets. Ice thickness is found from freeboard elevation assuming hydrostatic equilibrium and using a correction term for the firn air content (Supplementary Discussion 8 and Supplementary Fig. 5). This correction comes from a semi-empirical model using our regional climate model, RACMO2, and depth–density observations[31]. The velocity data are an InSAR mosaic over the 2007–2009 period[20]. The GLF is obtained using InSAR velocities and ice thicknesses at, or near, the grounding line. For 68% of the GLF, thicknesses from IPR data are used. Our grounding line is a new compilation to provide the most complete and accurate coverage (Supplementary Discussion 5). Our SMB is an average over 32 years (1979–2010) from RACMO2[6] (Supplementary Discussion 7 and Supplementary Figs 3 and 4). To include the 10% of ice-sheet area unsurveyed in our total calving and melt estimates, we use the SMB of these areas and apply a regionally differentiated melting and calving ratio to them (Supplementary Discussion 3 and Supplementary Fig. 6).

Online Content Any additional Methods, Extended Data display items and Source Data are available in the online version of the paper; references unique to these sections appear only in the online paper.

Received 3 April; accepted 7 August 2013.
Published online 15 September 2013.

1. Jacobs, S. S., Helmer, H. H., Doake, C. S. M., Jenkins, A. & Frolich, R. M. Melting of ice shelves and the mass balance of Antarctica. *J. Glaciol.* **38,** 375–387 (1992).
2. Orheim, O. in *Glaciers, Ice Sheets and Sea Level: Effect of a CO2-Induced Climatic Change* 210–215 (National Academic, 1985).
3. Jenkins, A. & Doake, C. S. M. Ice-ocean interaction on Ronne Ice Shelf, Antarctica. *J. Geophys. Res.* **96,** 791–813 (1991).
4. Rignot, E. & Jacobs, S. S. Rapid bottom melting widespread near Antarctic ice sheet grounding lines. *Science* **296,** 2020–2023 (2002).
5. Joughin, I. & Padman, L. Melting and freezing beneath Filchner-Ronne Ice Shelf, Antarctica. *Geophys. Res. Lett.* **30,** 1477 (2003).
6. Lenaerts, J. T. M., van den Broeke, M. R., van de Berg, W. J., van Meijgaard, E. & Kuipers Munneke, P. A new, high-resolution surface mass balance map of Antarctica (1979–2010) based on regional atmospheric climate modeling. *Geophys. Res. Lett.* **39,** L04501 (2012).
7. Silva, T. A. M., Bigg, G. R. & Nicholls, K. W. Contribution of giant icebergs to the Southern Ocean freshwater flux. *J. Geophys. Res.* **111,** C03004 (2006).
8. Pritchard, H. D. *et al.* Antarctic ice-sheet loss driven by basal melting of ice shelves. *Nature* **484,** 502–505 (2012).
9. Pritchard, H. D., Arthern, R. J., Vaughan, D. G. & Edwards, L. A. Extensive dynamic thinning on the margins of the Greenland and Antarctic ice sheets. *Nature* **461,** 971–975 (2009).
10. Dupont, T. K. & Alley, R. B. Assessment of the importance of ice-shelf buttressing to ice-sheet flow. *Geophys. Res. Lett.* **32,** L04503 (2005).
11. De Angelis, H. & Skvarca, P. Glacier surge after ice shelf collapse. *Science* **299,** 1560–1562 (2003).
12. Doake, C. S. M. & Vaughan, D. G. Rapid disintegration of the Wordie Ice Shelf in response to atmospheric warming. *Nature* **350,** 328–330 (1991).
13. Raiswell, R., Benning, L., Tranter, M. & Tulaczyk, S. Bioavailable iron in the Southern Ocean: the significance of the iceberg conveyor belt. *Geochem. Trans.* **9,** 7 (2008).
14. Yu, J., Liu, H., Jezek, K. C., Warner, R. C. & Wen, J. Analysis of velocity field, mass balance, and basal melt of the Lambert Glacier-Amery Ice Shelf system by incorporating Radarsat SAR interferometry and ICESat laser altimetry measurements. *J. Geophys. Res.* **115,** B11102 (2010).
15. Nicholls, K. W., Makinson, K. & Johnson, M. R. New oceanographic data from beneath Ronne Ice Shelf, Antarctica. *Geophys. Res. Lett.* **24,** 167–170 (1997).
16. Williams, M. J. M., Jenkins, A. & Determann, J. in *Ocean, Ice, and Atmosphere: Interactions at the Antarctic Continental Margin* 285–299 (Antarct. Res. Ser. 75, AGU, 1998).
17. Hellmer, H. H. Impact of Antarctic ice shelf basal melting on sea ice and deep ocean properties. *Geophys. Res. Lett.* **31,** L10307 (2004).
18. Timmermann, R., Wang, Q. & Hellmer, H. H. Ice-shelf basal melting in a global finite-element sea-ice/ice-shelf/ocean model. *Ann. Glaciol.* **53** (2012).
19. Griggs, J. A. & Bamber, J. L. Antarctic ice-shelf thickness from satellite radar altimetry. *J. Glaciol.* **57,** 485–498 (2011).
20. Rignot, E., Mouginot, J. & Scheuchl, B. Ice flow of the Antarctic ice sheet. *Science* **333,** 1427–1430 (2011).
21. King, M. A. *et al.* Lower satellite-gravimetry estimates of Antarctic sea-level contribution. *Nature* **491,** 586–589 (2012).
22. Hellmer, H. H., Kauker, F., Timmermann, R., Determann, J. & Rae, J. Twenty-first-century warming of a large Antarctic ice-shelf cavity by a redirected coastal current. *Nature* **485,** 225–228 (2012).
23. Potter, J. R., Paren, J. G. & Loynes, J. Glaciological and oceanographic calculations of the mass balance and oxygen isotope ratio of a melting ice shelf. *J. Glaciol.* **30,** 161–170 (1984).
24. Fricker, H. A., Popov, S., Allison, I. & Young, N. Distribution of marine ice beneath the Amery Ice Shelf. *Geophys. Res. Lett.* **28,** 2241–2244 (2001).
25. Holland, P. R., Corr, H. F. J., Vaughan, D. G., Jenkins, A. & Skvarca, P. Marine ice in Larsen ice shelf. *Geophys. Res. Lett.* **36,** L11604 (2009).
26. Zotikov, I. A., Zagorodnov, V. S. & Raikovsky, J. V. Core drilling through the Ross ice shelf (Antarctica) confirmed basal freezing. *Science* **207,** 1463–1465 (1980).
27. Whitehouse, M. J. *et al.* Substantial primary production in the land-remote region of the central and northern Scotia Sea. *Deep-Sea Res. II* **59–60,** 47–56 (2012).
28. Alderkamp, A.-C. *et al.* Iron from melting glaciers fuels phytoplankton blooms in the Amundsen Sea (Southern Ocean): phytoplankton characteristics and productivity. *Deep-Sea Res. II* **71–76,** 32–48 (2012).
29. Smith, K. L. *et al.* Free-drifting icebergs: hot spots of chemical and biological enrichment in the Weddell Sea. *Science* **317,** 478–482 (2007).
30. Zwally, H. J. *et al.* Mass changes of the Greenland and Antarctic ice sheets and shelves and contributions to sea-level rise: 1992–2002. *J. Glaciol.* **51,** 509–527 (2005).
31. Ligtenberg, S. R. M., Helsen, M. M. & van den Broeke, M. R. An improved semi-empirical model for the densification of Antarctic firn. *Cryosphere* **5,** 809–819 (2011).

Supplementary Information is available in the online version of the paper.

Acknowledgements This work was supported by funding from the ice2sea programme of the European Union Seventh Framework Programme, grant number 226375. This work is ice2sea contribution number 139. M.R.v.d.B., J.T.M.L. and S.R.M.L. acknowledge funding from the Netherlands Polar Programme. J.L.B. was supported by NERC grant NE/I027401/1.

Author Contributions M.A.D. produced the results, led the development of the study and wrote the manuscript. J.L.B. had the idea for the study and contributed to the development of the methods, to the discussion of results and, extensively, to writing the manuscript. J.A.G. produced the calving-front elevation error and provided the ice-shelf elevation. J.T.M.L. and M.R.v.d.B. provided the SMB data and error analysis. S.R.M.L. and M.R.v.d.B. provided the firn data and error analysis. G.M. provided the grounding-line and ice-shelf mask data and discussion. All authors commented on the manuscript.

Author Information Reprints and permissions information is available at www.nature.com/reprints. The authors declare no competing financial interests. Readers are welcome to comment on the online version of the paper. Correspondence and requests for materials should be addressed to M.A.D. (mathieu.depoorter@bristol.ac.uk) or J.L.B. (j.bamber@bristol.ac.uk).

METHODS

Budget analysis. We use standard mass budget methods to calculate the basal mass balance for each ice shelf in Antarctica, following $0 = \mathrm{BMB} + \mathrm{SMB} + \mathrm{GLF} - \mathrm{CF}$. We determine BMB as the remaining unknown of the mass balance equation, assuming a steady state. Ice-shelf thinning rates[8] are added to BMB to account for non-steady-state behaviour. Our ice-shelf thickness data set does not include shelves smaller than 100 km^2 (ref. 19). Therefore, no GLF or CF is calculated for those shelves. To include this unsurveyed 10% of the total ice-sheet area in our total calving and melting numbers, we use the surface mass balance[6] of these areas and apply a physically based regional melting and calving ratio to them (Supplementary Discussion 3 and Table 6).

Calving fluxes. The calving flux is found by integrating ice-shelf thickness and ice velocity along the calving front. The calving front has been tracked following the coastline close to the ice front, but 2–10 km inland to avoid interpolation artefacts at the ice–ocean boundary (Supplementary Fig. 2), using a combined 1-km-resolution mask of both ice-shelf thickness[19] and velocity data[20]. Our 1-km-gridded ice-shelf thickness is based on 1994–1995 altimetry data from ERS-1 and supplemented by ICESat data from south of the ERS-1 limit[19]. Elevations are corrected to the year 2009 using elevation rates from ERS-1[30] (1994–2002) and from ICESat[8] (2003–2009) to be consistent with velocity and IPR data. Thickness is found from freeboard elevation assuming hydrostatic equilibrium and using a correction term for the firn layer. The firn correction stems from a semi-empirical model using the regional atmospheric climate model RACMO2 and depth–density observations[31]. The velocity data set is an InSAR mosaic over the 2007–2009 period[20]. A sensitivity analysis for the calving-flux gate placement is provided in Supplementary Discussion 6.

Grounding lines and grounding-line fluxes. Our grounding-line data set is a compilation of published grounding lines (mainly from InSAR, but also complemented with imagery and ICESat) to achieve complete coverage and the most accurate and up-to-date delineations (Supplementary Discussion 5). The GLF is obtained using InSAR velocities and ice thicknesses close to the grounding line. We use surface-elevation-derived thicknesses for 32% of the GLF. For the remainder, we use IPR-derived thicknesses from various campaigns for the years 2009–2012 (Supplementary Table 1). IPR tracks are chosen just upstream of the grounding line (rather than downstream) to avoid the strong melting at the grounding line, and SMB is used to correct for the small area in between.

Surface mass balance. For our SMB, we use the average of 32 years (1979–2010) of SMB from RACMO2[6] run at a resolution of 27 km (Supplementary Fig. 3). This model takes into account drifting snow processes and is forced by the ERA-Interim reanalyses from the European Centre for Medium-Range Weather Forecasts. Islands and ice rises located within ice shelves are included in the ice-shelf mask[19] for SMB calculation under the assumption that net surface accumulation equals GLF for those features. There is no statistically significant temporal trend in SMB over the ice shelves[6].

Error assessment. The error assessment is done separately for each ice shelf (Fig. 1 and Supplementary Table 1). ICESat points within a zone extending 10 km upstream of the calving front are used to assess the calving-flux elevation error at the calving front of each ice shelf. To account for the time difference between the ERS-1 (1994–95) and the ICESat data (2003–2009), a $\mathrm{d}h/\mathrm{d}t$ correction is applied following $\mathrm{d}h/\mathrm{d}t$ trends in ERS-1 and ERS-2 for the period 1992–2001[30]. The grounding-line thickness error is assumed to be 10 m for IPR tracks. We estimate a 28% error for ice-shelf SMB and a 10% error for the firn air content correction (Supplementary Discussion 7 and 8 and Supplementary Figs 4 and 5). Errors in ice thickness derived from ice-penetrating radar, ice surface velocity, SMB and firn correction for each shelf are assumed to be uncorrelated. For SMB, this is supported by the spread of points around the least-squares linear fit shown in Supplementary Fig. 4. A random error of 3% is included in the calving-flux error to account for gate placement (Supplementary Discussion 6). In determining the total calving-flux error, we assumed that the error in surface elevation (which affects the ice thickness error) is correlated between ice shelves, because it seems to be systematic at a regional level[19]. For the GLF derived from surface elevation and the assumption of hydrostatic equilibrium, the error in thickness is found to be 10–15% in the vicinity of the grounding line[19], with both positive and negative differences. We assume an uncertainty in GLF of 20% for these areas. The error in GLF introduced from the interpolation of unsurveyed areas is determined from the root mean squared SMB error and a 10% deviation from balance for the grounded ice sheet. This is supported by the fact that elevation rates from altimetry for these unsurveyed sectors are small and they are in areas of slow flow, where changes in ice dynamics are expected to be limited[9]. The standard deviation of the differences in melt ratio between shelves experiencing similar oceanic conditions (Supplementary Discussion 3) is used as a measure of the uncertainty in partitioning the interpolated GLF between calving and BMB for the unsurveyed sectors.

Data description. The data produced for this paper are ice-shelf ice thickness and a continent-wide grounding line. These data sets can be found at http://pangaea.de/. The other data sets used in this study can be found at the following websites: http://nsidc.org/data/docs/measures/nsidc0484_rignot/ (ice velocity field), http://nsidc.org/data/icebridge/ and https://data.cresis.ku.edu/ (IPR ice thickness), http://nsidc.org/data/atlas/news/antarctic_coastlines.html (MOA grounding line and coastline), http://nsidc.org/data/docs/agdc/nsidc0469_brunt/ (ICESat grounding-line points), http://nsidc.org/data/docs/agdc/nsidc0489_bindschadler/ (ASAID project grounding line), http://nsidc.org/data/docs/measures/nsidc0498_rignot/ (DInSAR grounding line), http://nsidc.org/data/nsidc-0280.html (MOA mosaic), http://nsidc.org/data/radarsat/ramp_basics/mosaic_5kmw.html (RAMP mosaic) and http://lima.nasa.gov/ (LIMA mosaic).